Characterization of the α−β Phase Transition in Friedels Salt ($Ca_2Al(OH)_6Cl·2H_2O$) by Variable-Temperature ^{27}Al MAS NMR Spectroscopy

Morten Daugaard Andersen, Hans J. Jakobsen, and Jørgen Skibsted*

Instrument Centre for Solid-State NMR Spectroscopy, Department of Chemistry, University of Aarhus, DK-8000 Aarhus C, Denmark

Received: December 18, 2001; In Final Form: April 30, 2002

The first application of variable-temperature ^{27}Al MAS NMR spectroscopy to the satellite transitions in the characterization of a structural phase transition is presented by an investigation of Friedels salt ($Ca_2Al(OH)_6Cl·2H_2O$) over the temperature range from −121 to 109 °C. Accurate values for the ^{27}Al quadrupole coupling parameters (C_Q and η_Q) and the isotropic chemical shifts are obtained from either the manifold of spinning sidebands for the satellite transitions or the line shape observed for the central transition. These data demonstrate that the quadrupole coupling parameters clearly reflect the structural α−β phase transition for Friedels salt at about 34 °C, whereas the isotropic chemical shift is invariant over the studied temperature range. The variations in C_Q and η_Q with temperature show a parabolic decrease in C_Q and an increase in η_Q with increasing temperature for the α form of Friedels salt, while only a small linear decrease in C_Q with increasing temperature and a temperature-independent value for η_Q are observed for the β form. The nonlinear variations of C_Q and η_Q with temperature for the α form and their relationships with changes in the structural parameters associated with thermal expansion of the unit cell are discussed. Finally, the abrupt changes in C_Q and η_Q at the temperature for the phase transition are investigated by point-monopole calculations of the ^{27}Al electric-field gradient tensor, which strongly suggest that hydrogen bonding plays an important role in the structural changes that occur during the phase transition.

Introduction

The migration of chloride ions into concrete has an important impact on the lifetime of reinforced concrete structures because these ions may break down the passive film of γ-Fe_2O_3 on the steel reinforcement and cause the formation of rust.[1,2] This process is associated with an increase in volume, which results in cracking of the concrete. Chloride ions in concrete may be present as free chloride ions in the pore water, physically adsorbed Cl^- ions on the surface of the amorphous calcium−silicate−hydrate (C−S−H) gel, and ionically bonded Cl^- ions in Friedels salt $[Ca_2Al(OH)_6]Cl·2H_2O$.[1,2] The formation of Friedels salt may reduce the damaging effects of chloride ions in concrete, because it has been proposed that its aluminum-containing hydration products react with Cl^- ions from the pore water and form Friedels salt.[3,4] Thus, the chemical binding of chloride ions in this phase reduces the concentration of Cl^- in the pore water and Cl^- ions physically adsorbed on the C−S−H gel. Thereby, the deleterious reaction of the chloride ions with the steel reinforcement is suppressed.[3,5,6]

The structures for the two polymorphs of Friedels salt,[7,8] illustrated in Figure 1 for the β polymorph, consist of principal layers with the composition $[Ca_2Al(OH)_6]^+$.[9] Because of the stacking of the principal layers, the water molecule bonded to the seven coordinated Ca^{2+} ions forms octahedral cavities in the interlayer.[7,8] Charge balance is achieved when Cl^- ions are introduced into these cavities. The mechanism for the incorporation of Cl^- ions is not well understood. However, it has been proposed that the Cl^- ions in the pore water either enter directly into the octahedral cavities during the formation of Friedels salt or are incorporated by an anion-exchange mechanism in which Cl^- substitute for OH^-, resulting in a release of hydroxyl ions

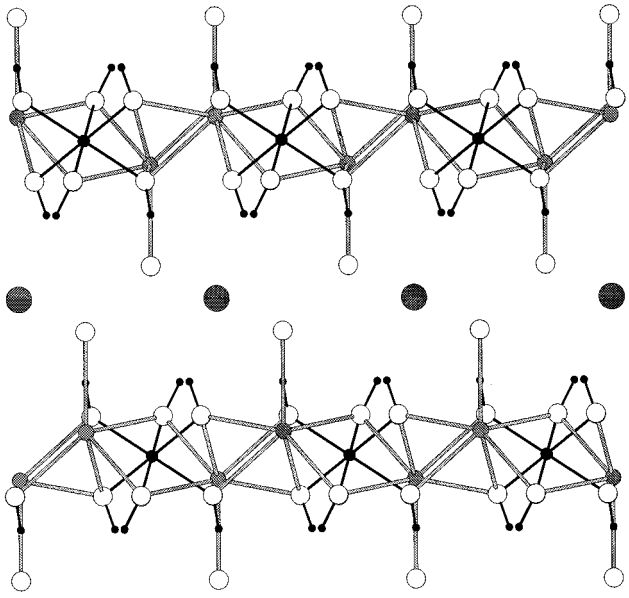

Figure 1. Perspective representation of the layered structure for the β phase of Friedels salt based on the data from the reported single-crystal XRD structure[8] and shown as a projection along the [010] direction. The plot illustrates the octahedral coordination of Al (medium filled circles) to six hydroxyl groups (small filled circles for H and large open circles for O) and the seven coordinated Ca^{2+} ions (medium shaded circles). The water molecules in the interlayer are bonded to the Ca^{2+} ions, thereby forming the octahedral cavities where the Cl^- anions (large shaded circles) are located. For clarity, the hydrogens of the water molecules are omitted.

* To whom correspondence should be addressed. Phone: (+45) 89423900. Fax: (+45) 86196199. E-mail: jskib@chem.au.dk.

10.1021/jp014573p CCC: $22.00
Published on Web 06/21/2002

to the pore solution.[3] Furthermore, it is known that Friedels salt undergoes a phase transition at about 34 °C from a low-temperature α form (monoclinic, space group $C2/c$)[7] to a high-temperature β phase (rhombohedral, space group $R\bar{3}c$).[8] From the single-crystal X-ray diffraction studies of both forms, it is apparent that the phase transition is strongly related to the Cl^- ions in the interlayer cavities.[7,8] Other lamellar calcium aluminate hydrates have charge-balancing anions such as NO_3^- [10] and CO_3^{2-} [11], which are directly bonded to the Ca^{2+} ions in its seven coordination sphere of the Ca^{2+} ions in the principal layers. Thus, the structures of these compounds are quite different from Friedels salt in which the Cl^- ions are situated in the interlayer cavities.

This work presents a variable-temperature (VT) ^{27}Al magic-angle spinning (MAS) NMR study of Friedels salt over a temperature range from −121 to 109 °C. The VT MAS NMR spectra of the central and satellite transitions allow a precise determination of the ^{27}Al quadrupole coupling parameters (C_Q and η_Q), which reflect the electric-field gradients (EFGs) at the nuclear site and thereby the local Al environment. The results demonstrate that the variation with temperature of these parameters clearly reflect the α−β phase transition for Friedels salt and that C_Q and η_Q are much more sensitive structural probes as compared to the ^{27}Al isotropic chemical shift (δ_{iso}). These results may find use in ^{27}Al VT MAS NMR studies to detect and characterize Friedels salt in complex cement mixtures. Furthermore, the structural implications of the significant difference in C_Q and η_Q for the α and β form are investigated by point-monopole calculations of the ^{27}Al EFG tensors and suggest that hydrogen bonding has an important impact on the phase transition.

^{27}Al VT NMR has earlier been used in studies of temperature effects and phase transitions for several types of inorganic materials employing either ^{27}Al single-crystal or static-powder NMR. These include investigations of (i) the temperature dependence of the quadrupolar coupling parameters for alums ($MAl(SO_4)_2 \cdot 12H_2O$, M = NH_4, Na, K, Rb, Tl)[12−14] and $YAlO_3$,[15] (ii) the α−β phase transition for $AlPO_4$-cristobalite,[16] and (iii) relaxation studies for a single crystal of emerald ($Be_3Al_2Si_6O_{18}$:Cr^{3+}).[17] Furthermore, high-temperature ($800 < T < 2000$ K) equipment has been developed[18] for studying the dynamics and crystallization processes of inorganic liquids and glasses.[19] ^{27}Al VT MAS NMR has only been used in a few cases and only to detect structural changes via observation of the central transition.[16] Thus, the present work represents the first investigation in which the complete manifold of spinning sidebands (ssbs), observed in ^{27}Al MAS spectra of the satellite transitions, is used to follow a structural phase transition.

Experimental Section

Friedels salt was prepared in a CO_2-free environment by hydrothermal synthesis using boehmite (AlOOH), $CaCl_2 \cdot 2H_2O$, $Ca(OH)_2$, and demineralized water (triple-distilled water), following the procedure by Terzis et al.[7] The synthesis employed the following molar ratios for the reagents: 2.0 Al(OOH)/1.10 $CaCl_2 \cdot 2H_2O$/2.97 $Ca(OH)_2$/233 H_2O. After mixing the reagents for 15 min, the mixture was heated in a Teflon-lined autoclave at 220 °C for 72 h. The product was washed with demineralized water and dried in a desiccator at room temperature. The dry sample was kept in an airtight container to prevent contamination from CO_2. The basic structure and purity of the sample was confirmed by powder X-ray diffraction.

^{27}Al VT MAS NMR experiments were performed on a Varian INOVA-300 (7.1 T) spectrometer using a home-built, narrow-bore VT CP/MAS NMR probe for 7 mm o.d. rotors. The probe is capable of operating in the temperature range from −150 to 210 °C by regulating the temperature of the air-bearing gas employing a home-built VT heater/controller unit based on a CAL 3200 microprocessor as described elsewhere.[20] The low-temperature work used pressurized N_2 gas, which was pre-cooled by passing through a heat exchanger in a liquid N_2 dewar. The temperature gradient across the rotor volume is less than 2 °C, and the actual sample temperature was determined using ^{207}Pb MAS NMR of $Pb(NO_3)_2$ as a NMR thermometer,[21] using a temperature coefficient of 0.758 ppm/°C determined in our laboratory. Slices of $NaNO_3$, packed above/below the sample of Friedels salt in the rotor, allowed an accurate setting of the magic angle at each temperature by minimization of the line widths observed for the ^{23}Na satellite transitions. All ^{27}Al VT MAS NMR spectra employed single-pulse excitation with a pulse width of 1.0 μs for a rf field strength of $\gamma B_1/(2\pi) = 42$ kHz, ^{1}H decoupling with $\gamma B_2/(2\pi) = 45$ kHz, a relaxation delay of 2 s, a spinning speed of $\nu_r = 5.0$ kHz regulated to ±1 Hz by the Varian spinning-speed controller, and typically 2048 scans. ^{27}Al isotropic chemical shifts are in ppm relative to an external sample of 1.0 M $AlCl_3 \cdot 6H_2O$. Simulations of the solid-state ^{27}Al MAS NMR spectra were performed on a SUN ULTRA 5 workstation using the STARS solid-state NMR software package.[22]

Results and Discussion

The α Phase of Friedels Salt. The low-temperature α phase of Friedels salt is investigated by ^{27}Al VT MAS NMR over a temperature range from −121 to 28 °C by the analysis of 19 experimental spectra. The appearances of the ^{27}Al MAS spectra in this temperature range are quite similar and an illustrative spectrum ($T = -3$ °C) is shown in Figure 2a. This spectrum shows the manifold of ssbs from the ^{27}Al satellite transitions, which are observed over a spectral width of approximately 1 MHz. The insets in Figure 2a illustrate that each ssb is partly split into two resonances, one from the inner ($m = \pm 1/2 \leftrightarrow m = \pm 3/2$) and one from the outer ($m = \pm 3/2 \leftrightarrow m = \pm 5/2$) satellite transitions, which reflect the difference in second-order quadrupolar shift for these transitions. We note that the narrow line width of the ssbs from the inner satellite transitions (fwhm ≈ 240 Hz) and the resolution of the ssbs from the inner and outer satellite transitions are only observed when ^{1}H decoupling is employed. Furthermore, the narrow line widths and the splitting for the ssbs demonstrate that our sample of Friedels salt is highly crystalline. Least-squares fitting of simulated to experimental intensities for the manifold of ssbs (Figure 2a) gives the quadrupole coupling parameters $C_Q = 1.49 \pm 0.03$ MHz and $\eta_Q = 0.89 \pm 0.02$, where the error limits (95% confidence intervals) have been determined using the method described elsewhere.[23] The optimized simulation, including all transitions and the second-order term of the average Hamiltonian for the quadrupolar interaction,[22] is illustrated in Figure 2b and reproduces convincingly the spectral features of the experimental spectrum. The observation of resonances from a single ^{27}Al site with an isotropic chemical shift of $\delta_{iso} = 9.2 \pm 0.3$ ppm is in agreement with the crystal structure for the α phase,[7] which contains an unique, octahedrally coordinated Al site in the asymmetric unit. Furthermore, the strong effects of ^{1}H decoupling on the line widths of the ssbs in the experimental spectra reflect the fact that Al is coordinated to six OH^- groups.

The 19 ^{27}Al VT MAS NMR spectra of the satellite transitions for the α form have been analyzed in a similar manner as the spectrum in Figure 2a. ^{27}Al quadrupole coupling parameters and

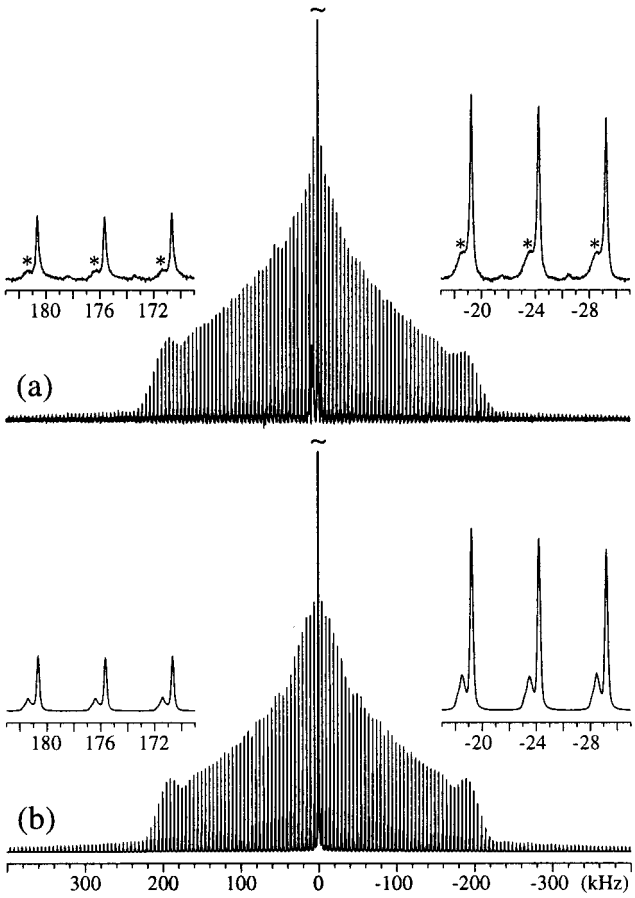

Figure 2. Experimental (a) ^{27}Al MAS NMR spectrum ($\nu_r = 5.0$ kHz, 1024 scans) illustrating the manifold of ssbs from the satellite transitions for the low-temperature α form of Friedels salt at $T = -3$ °C and optimized simulation (b) of the manifolds of ssbs in panel a employing the parameters $C_Q = 1.49$ MHz, $\eta_Q = 0.89$, and $\delta_{iso} = 9.4$ ppm. The insets are expansions of the line shapes for the individual ssbs, which illustrate that the ssbs from the inner and outer satellite transitions are partly resolved. The asterisks indicate the ssbs from the outer satellite transitions.

TABLE 1: ^{27}Al Quadrupole Coupling Constants (C_Q), Asymmetry Parameters (η_Q), and Isotropic Chemical Shifts (δ_{iso}) for Friedels Salt at 12 Selected Temperatures

T (°C)	C_Q (MHz)	η_Q	δ_{iso} (ppm)
−121	1.58 ± 0.03^a	0.80 ± 0.02^a	9.1 ± 0.3^b
−98	1.56	0.80	9.2
−64	1.55	0.82	9.2
−30	1.52	0.84	9.3
−3	1.49	0.89	9.4
18	1.42	0.93	9.2
28	1.40	0.98	9.5
38	1.09 ± 0.04	0.04 ± 0.05	9.1
41	1.07 ± 0.02	0.00 ± 0.05	9.1
66	1.06 ± 0.02	0.03 ± 0.03	9.2
92	1.06 ± 0.02	0.01 ± 0.04	9.3
109	1.05 ± 0.02	0.03 ± 0.05	9.4

[a] The error limits (95% confidence intervals) for C_Q and η_Q are ±0.03 MHz and ±0.02, respectively, for all parameters determined for the α-form. [b] The error limit for δ_{iso} is estimated to ±0.3 ppm for all temperatures.

isotropic chemical shifts from these analyses are listed in Table 1 for seven selected temperatures. The ^{27}Al NMR data have also been confirmed by optimization of simulated to experimental second-order quadrupolar line shapes for the central ($m = {}^1/_2 \leftrightarrow m = -{}^1/_2$) transition. As an example, Figure 3a shows the spectrum of the ^{27}Al central transition for $T = -121$ °C

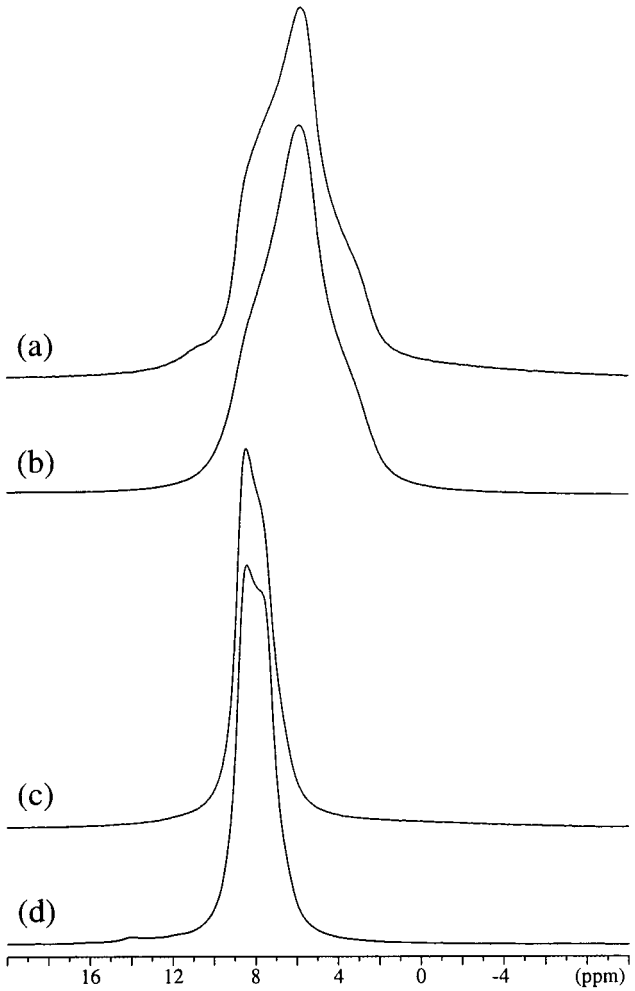

Figure 3. Experimental ^{27}Al VT MAS NMR spectra ($\nu_r = 5.0$ kHz, 256 scans) illustrating the line shape of the central transition for (a) the α phase at −121 °C and (c) the β phase of Friedels salt at 41 °C. The optimized simulations of the experimental line shapes in spectra a and c are shown in spectra b and d, respectively, and correspond to the parameters listed in Table 1 for $T = -121$ and 41 °C.

and Figure 3b the corresponding simulation. In accordance with earlier studies of compounds with rather small ^{27}Al quadrupole couplings, the highest precision for C_Q, η_Q, and δ_{iso} is obtained by analysis of the ssbs from the satellite transitions as compared to line shape simulations of the central transition.

The β Phase of Friedels Salt. By increasing the temperature in the ^{27}Al VT MAS experiments from 28 to 38 °C, an abrupt change in the experimental spectra is observed. The line width for the central transition becomes significantly narrower at 38 °C, and the line shape adopts the spectral features of an axially symmetric ^{27}Al EFG tensor (i.e., $\eta_Q \approx 0$). These changes reflect the structural phase transition from the α to the β form of Friedels salt, in full agreement with the reported phase-transition temperature at about 33 °C.[7,8]

The line shapes of the central transition for the α and β phase are compared in Figure 3. The β form has been studied by 10 ^{27}Al VT MAS experiments in the range from 38 to 109 °C. All of these spectra exhibit a second-order quadrupolar line shape for a single ^{27}Al resonance similar to the spectrum in Figure 3c for $T = 41$ °C. However, the intensities of the ssbs from the satellite transitions are significantly reduced compared to those observed for the α form, preventing a determination of C_Q and η_Q from these transitions. This reduction in intensity is ascribed to the introduction of structural or dynamic disorder in the

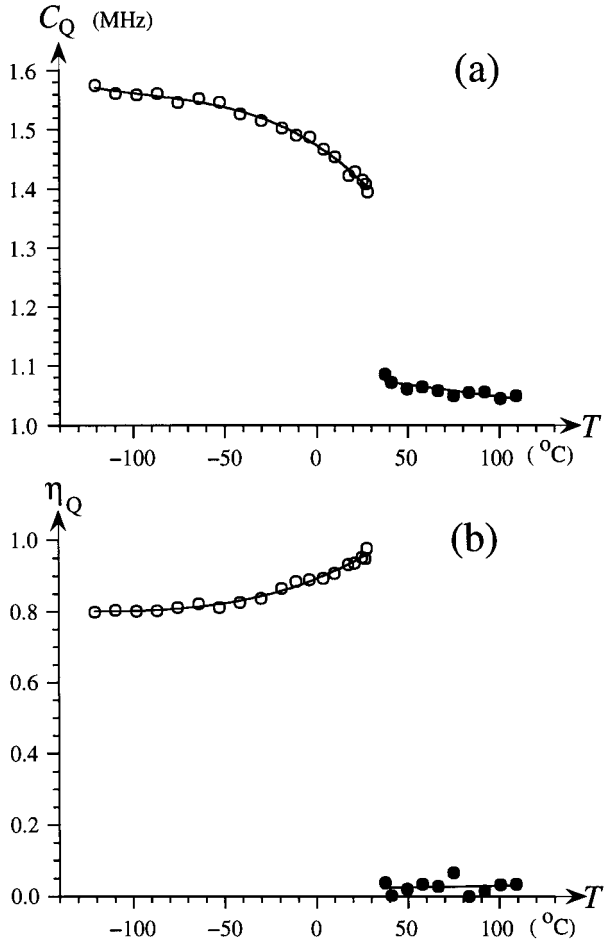

Figure 4. Graphs illustrating the temperature dependencies of the ^{27}Al quadrupole coupling parameters (a) C_Q and (b) η_Q for the α phase (open circles) and β phase (filled circles) of Friedels salt. The curves correspond to the results from regression analysis of the data for the α form employing a second-order polynomial (cf., eqs 1 and 2).

structure associated with the phase transition. Thus, C_Q, η_Q, and δ_{iso} have been determined from line shape analysis of the central transition for the β phase. Figure 3c,d compares experimental and simulated line shapes for the central transition at $T = 41$ °C, while optimized C_Q, η_Q, and δ_{iso} data for the β form at five selected temperatures are listed in Table 1. The observation of a single ^{27}Al resonance and an axially symmetric EFG tensor ($\eta_Q \approx 0$) are in agreement with the crystal structure reported for the β form, in which Al is situated on a 3-fold axis.[8]

Temperature Variation of the ^{27}Al Quadrupole Coupling Parameters. The ^{27}Al quadrupole coupling parameters, determined from the analysis of 29 VT MAS NMR spectra and summarized for 12 selected temperatures in Table 1, are shown as a function of temperature in Figure 4. The abrupt changes in C_Q and η_Q at about 34 °C demonstrate that these parameters are highly sensitive to the structural α−β phase transition at this temperature. From the VT MAS NMR spectra and the plots in Figure 4, we obtain the phase-transition temperature $T = 34 \pm 4$ °C, which is in good agreement with the temperature range 32.0−34.2 °C reported for the α−β transition from an XRD study.[8] It is noted that a phase-transition temperature of 6 °C has been reported for Friedels salt from differential scanning calorimetry and ^{35}Cl static-powder NMR,[24] however, for a sample in which chemical analysis indicated that 24% of the chloride anions were replaced by carbonate anions in the structure. This replacement may tentatively explain the lower phase-transition temperature observed in that work. Furthermore, it is observed that C_Q decreases with increasing temperature for the α form. This variation with temperature can be fitted to a second-order polynomial according to the equation

$$C_Q = (-9.35 \times 10^{-6}\ \text{MHz}\ ^\circ\text{C}^{-2})T^2 - (1.90 \times 10^{-3}\ \text{MHz}\ ^\circ\text{C}^{-1})T + 1.47\ \text{MHz} \quad (1)$$

with the correlation coefficient $R = 0.993$. A significant change in η_Q is also observed for the α form, which can be fitted to the second-order polynomial

$$\eta_Q = (1.02 \times 10^{-5}\ ^\circ\text{C}^{-2})T^2 + (1.95 \times 10^{-3}\ ^\circ\text{C}^{-1})T + 0.894 \qquad (R = 0.992) \quad (2)$$

For the β phase, our data indicate a minor decrease in C_Q with increasing temperature (Figure 4a and Table 1), whereas η_Q is found to be independent of temperature (Figure 4b) in agreement with the local symmetry for Al in the crystal structure. Furthermore, examination of the δ_{iso} values (Table 1) shows that this parameter is invariant ($\delta_{iso} = 9.3 \pm 0.3$ ppm) in the temperature range from −121 to 109 °C, demonstrating that δ_{iso} cannot be used to monitor the α to β phase transition around 30 °C. The invariance in δ_{iso} contrasts the ^{27}Al VT static-powder and MAS NMR study of the α−β phase transition for $AlPO_4$-cristobalite ($AlPO_4$-c, $T = 220$ °C) by Phillips et al.,[16] who observed a discontinuous decrease in δ_{iso} by −2 to −3 ppm on going from the α to the β form. However, for the low-symmetry α form of $AlPO_4$-c, these authors report a similar (although almost linear) decrease in C_Q with increasing temperature as observed for the α form of Friedels salt. A linear decrease in C_Q with increasing temperature has also been reported for ^{27}Al in $YAlO_3$,[15] whereas single-crystal ^{27}Al NMR studies of alums showed an increase in C_Q with increasing temperature for $MAl(SO_4)_2 \cdot 12H_2O$ (M = NH_4, K, Rb, Cs, Tl)[12,13] and a decrease in C_Q for increasing temperature for $NaAl(SO_4)_2 \cdot 12H_2O$.[14] These different temperature dependencies for alums have been investigated by Weiden and Weiss using point-monopole calculations of the effects from thermal vibrations on the ^{27}Al EFG tensors.[13,14] The calculations suggest that vibrations of Al^{3+} in the cages of sulfate ions lead to a decrease in C_Q with increasing temperature, whereas the vibrations of Al^{3+} in the $(H_2O)_6$ octahedra give an increase in C_Q with increasing temperature. For $NaAl(SO_4)_2 \cdot 12H_2O$, the sulfate groups are located considerably closer to the Al^{3+} ions as compared to the other alums, which may explain the negative temperature coefficient for Na-alum and the positive temperature coefficients for the remaining alums when the opposite vibrational effects from the $(H_2O)_6$ octahedron and the sulfate groups are taken into account.[13,14] For ionic crystals, it is predicted that C_Q decreases with increasing temperature when effects from the lattice expansion and the amplitude of the thermal motions are considered.[25] The ^{27}Al VT NMR results for the α phase of Friedels salt, $AlPO_4$-c,[16] and $YAlO_3$[15] are in agreement with this prediction.

The parabolic temperature dependencies of C_Q and η_Q for the α form of Friedels salt can alternatively be evaluated by calculation of the principal elements of the quadrupole coupling tensor (**Q**). In units of MHz, these elements are given by $Q_{zz} = C_Q$, $Q_{yy} = (^1/_2)C_Q(\eta_Q - 1)$, and $Q_{xx} = (-^1/_2)C_Q(\eta_Q + 1)$ using the convention $|Q_{zz}| \geq |Q_{xx}| \geq |Q_{yy}|$. Assuming a positive value for C_Q (Q_{zz}), these relations and the C_Q, η_Q data shown in Figure 4 give the temperature dependencies for Q_{yy} and Q_{xx} illustrated in Figure 5. The parabolic variations of C_Q and η_Q with temperature result in a similar temperature dependency for Q_{yy},

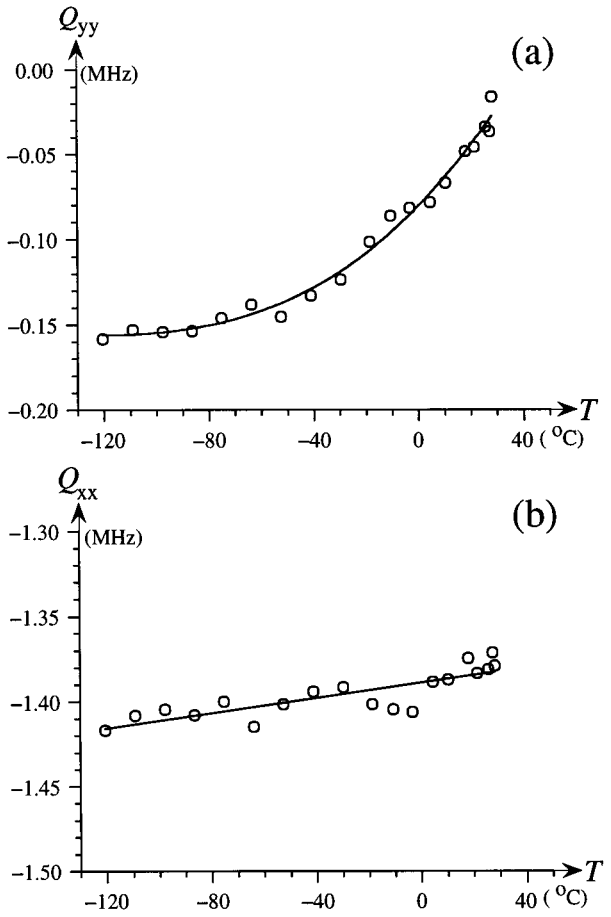

Figure 5. Plots of the principal elements (a) $Q_{yy} = (^1/_2)C_Q(\eta_Q - 1)$ and (b) $Q_{xx} = (^{-1}/_2)C_Q(\eta_Q + 1)$ of the ^{27}Al quadrupole coupling tensor versus temperature for the α form of Friedels salt, assuming a positive value for the quadrupole coupling constant (i.e., the Q_{zz} element). The results from regression analysis of the data in panels a and b are given in eqs 3 and 4, respectively.

which can be approximated by the second-order polynomial

$$Q_{yy} = (7.65 \times 10^{-6}\ \text{MHz}\ ^\circ\text{C}^{-2})T^2 + (1.54 \times 10^{-3}\ \text{MHz}\ ^\circ\text{C}^{-1})T - 0.08\ \text{MHz} \quad (R = 0.993) \quad (3)$$

In contrast, Figure 5b reveals that Q_{xx} is almost independent of temperature, considering the precision of our data, that is, $Q_{xx} = -1.42 \pm 0.04$ MHz for $T = -121$ °C and $Q_{xx} = -1.38 \pm 0.04$ MHz for $T = 28$ °C. However, linear regression of the data in Figure 5b gives the equation

$$Q_{xx} = (2.24 \times 10^{-4}\ \text{MHz}\ ^\circ\text{C}^{-1})T - 1.39\ \text{MHz} \quad (R = 0.830) \quad (4)$$

which indicates a very small linear variation with temperature for Q_{xx}. Similar results have recently been presented for ^{87}Rb in $RbClO_4$, in which linear relationships with temperature were observed for Q_{zz} (C_Q) and Q_{xx} whereas Q_{yy} exhibited a parabolic dependence.[26] Following the model calculations of the effects of thermal expansion on the Q_{ii} elements in that study,[26] the data for the α form of Friedels salt indicate that the temperature variation for the Q_{ii} elements are not solely a result of thermal expansion. Even an anisotropic thermal expansion, in which the crystallographic axes increase linearly with increasing temperature but with different temperature coefficients, should result in a linear variation of the Q_{ii} elements.[26] Thus, the parabolic variation observed for Q_{zz} and Q_{yy} for Friedels salt may reflect (i) an anisotropic thermal expansion in which the crystallographic axes do not vary linearly, (ii) other effects such as thermal vibrations having a marked influence on the ^{27}Al EFG tensor, or (iii) the thermal expansion being accompanied by rearrangements of the ions in the unit cell.

Point-Monopole Calculations. The significant changes in C_Q and η_Q associated with the α−β phase transition have been investigated by point-monopole calculations of the ^{27}Al EFG tensors, employing a similar approach as that recently used in studies of quadrupolar nuclei for other inorganic systems (e.g., ^{23}Na, ^{133}Cs, and ^{51}V)[23,27,28] and using the structural data reported for the α form (25 °C) and the β form (37 °C) of Friedels salt.[7,8] These calculations give the principal elements (V_{zz}^{calc}) of the ^{27}Al EFG tensor employing the definition $|V_{zz}^{calc}| \geq |V_{xx}^{calc}| \geq |V_{yy}^{calc}|$. The unique tensor element is proportional to the quadrupole coupling constant ($C_Q = (1 - \gamma_\infty)eQV_{zz}^{calc}/h$, where Q is the quadrupole moment for ^{27}Al), while the asymmetry parameter is calculated as $\eta_Q^{calc} = (V_{xx}^{calc} - V_{yy}^{calc})/V_{zz}^{calc}$. However, a precise value for the Sternheimer antishielding factor (γ_∞)[29] for ^{27}Al is not available, and thus, we have chosen to compare the experimental C_Q values with V_{zz}^{calc} in the evaluation of the relative magnitude of the quadrupole couplings for the α and β form of Friedels salt. For the single-crystal X-ray diffraction structure analysis of the α form, the positions of the H atoms were included as variable parameters in the refinement.[7] This resulted in O−H distances of 0.72 (O2−H2), 0.75 (O1−H1), and 0.77 Å (O3−H3) for the three different hydroxyl groups that constitute the $Al(OH)_6$ unit. Obviously, these distances are too short as a result of the nonspherical nature of the hydrogen atom electron density.[30] For the β form, the O−H distance for the hydroxyl group was restrained to 0.95(1) Å,[8] which is a significantly more realistic O−H distance as compared to those reported for the α form. We note that a O−H bond length of 0.924 Å has recently been reported for hydrogarnet ($Ca_3[Al(OH)_6]_2$) from a neutron diffraction study.[31] The O−H distances have a significant impact on the effective oxygen charges that are used in the point-monopole calculations. These charges are obtained from the covalences of the oxygen−cation bonds, which are calculated from the equations of Brown and Shannon[32] and from the chemical bond data of Brown and Altermatt.[33] Thus, as the first approach, we have recalculated the atomic coordinates for the hydrogen atoms of the α form (from the reported internuclear O−H vectors)[7] to obtain O−H distances of 0.95 Å for the three different hydroxyl groups. Employing these modified data for the α phase in point-monopole calculations of the ^{27}Al EFG tensors give the data $V_{zz}^{calc} = 0.271 \times 10^{21}$ V m^{-2}, $\eta_Q^{calc} = 0.04$ for the α form and $V_{zz}^{calc} = 0.259 \times 10^{21}$ V m^{-2}, $\eta_Q^{calc} = 0.00$ for the β form, when only the nearest oxygen coordination sphere for Al (i.e., an AlO_6 unit) is considered in the calculations. The almost identical values of V_{zz}^{calc} and η_Q^{calc} for the α and β forms from these calculations indicate that the nearest coordination sphere of Al is only slightly affected by the phase transition.

From the crystal structures, it is apparent that the environments of the chloride anion change significantly during the phase transition. Thus, the Al environment in the point-monopole calculations has been extended to a cluster of the 74 nearest atoms including the six nearest Cl^- anions. Again, the effective charges (q) of the individual atoms are estimated from the covalences of the oxygen−cation bonds, assuming (i) $q(Cl) = -1e$, (ii) effective charges for the O and H atoms of the water molecule, which give an electrically neutral H_2O molecule, and (iii) balanced charges for the cations corresponding to an

electrically neutral $Ca_2Al(OH)_6Cl$ unit. Furthermore, for the α form, recalculated H coordinates that give O−H distances of 0.95 Å are employed for the hydroxyl groups and the water molecule. For the α form, this procedure results in the following effective charges: $q(Al) = 2.008e$, $q(Ca) = 1.499e$, $q(O1) = -1.199e$, $q(O2) = -1.179e$, $q(O3) = -1.203e$, $q(OW) = -0.953e$, $q(HO1) = q(HO2) = q(HO3) = 0.526e$, $q(HWA) = q(HWB) = 0.463e$, and $q(Cl) = -1e$, using the same indices of the atoms as in the XRD structure analysis.[7] Employing these charges for the α form and the cluster of 74 atoms gives the values $V_{zz}^{calc} = 0.229 \times 10^{21}$ V m^{-2} and $\eta_Q^{calc} = 0.18$. The same approach for the β phase (cluster of 74 atoms) results in the parameters $V_{zz}^{calc} = 0.303 \times 10^{21}$ V m^{-2} and $\eta_Q^{calc} = 0.00$, using the effective charges $q(Al) = 2.017e$, $q(Ca) = 1.427e$, $q(O) = -1.151e$, $q(O_w) = -1.019e$, $q(H) = 0.506e$, $q(H_w) = 0.510e$, and $q(Cl) = -1e$. Again, the calculated values for V_{zz}^{calc} and η_Q^{calc} are very similar for the α and β form, and thus, they cannot explain the significant experimental change in C_Q and especially η_Q associated with the phase transition.

So far, the calculations have assumed identical O−H bond distances for the hydroxyl groups in the α form, although the XRD study indicated three different distances for the hydroxyl groups of the $Al(OH)_6$ unit.[7] Although these distances are too short, the XRD analysis strongly indicates that these bond distances vary as a result of hydrogen bonding to the chloride anion and the oxygen of the water molecule. This effect is investigated by implementing a systematic decrease of the shortest (O2−H2) and increase of the longest (O3−H3) O−H distance around 0.95 Å for a fixed value of 0.95 Å for the O1−H1 bond distance in the calculations. This results in the variation of V_{zz}^{calc} and η_Q^{calc} with increasing difference in O−H bond length ($\Delta d = d_{O3-H3} - d_{O2-H2}$) shown in Figure 6, parts a and b, respectively, for calculations considering only the nearest coordination sphere as well as the cluster of 74 atoms. For each calculation, the atomic coordinates of H2 and H3 are determined from the O2−H2 and O3−H3 internuclear vectors and, subsequently, the effective charges of the individual atoms using the procedure described above. The plots in Figure 6 show that an increasing difference in O−H distance for O2 and O3 results in an increase in V_{zz}^{calc} as well as η_Q^{calc} for both Al environments. The most marked effect for η_Q^{calc} is observed for the cluster of 74 atoms, which may reflect the fact that these calculations also include effects from the positions of the displaced H atoms and not only effects on the effective charges of the oxygen atoms as for the AlO_6 calculations. Furthermore, for a displacement of H2 and H3 by $d_{O3-H3} - d_{O2-H2} = 0.06$ Å, an asymmetry parameter $\eta_Q^{calc} = 0.93$ is calculated for the cluster of 74 atoms, which is very close to the experimental value for the α form at 28 °C. We note that this calculated value should be compared with the experimental data at this temperature, because the calculations employ the structural data determined from XRD at 25 °C.[7] The increase in V_{zz}^{calc} with increasing $d_{O3-H3} - d_{O2-H2}$ is also in agreement with the experimental values for C_Q of the α form, although the experimental ratio for C_Q(α phase)/C_Q(β phase) of about 1.3 is not reached for the calculated V_{zz}^{calc} values for the α and β phases. Thus, the calculated η_Q^{calc} and V_{zz}^{calc} values in Figure 6 strongly suggest that hydrogen bonding, reflected by a change in O−H distances for the hydroxyl groups, plays an important role in the structural rearrangements that occur during the phase transition. Thereby, these changes may account for the variations in the local environment of the Al atom that allow the clear observation of the α−β phase transition by the abrupt change in ^{27}Al quadrupole coupling parameters.

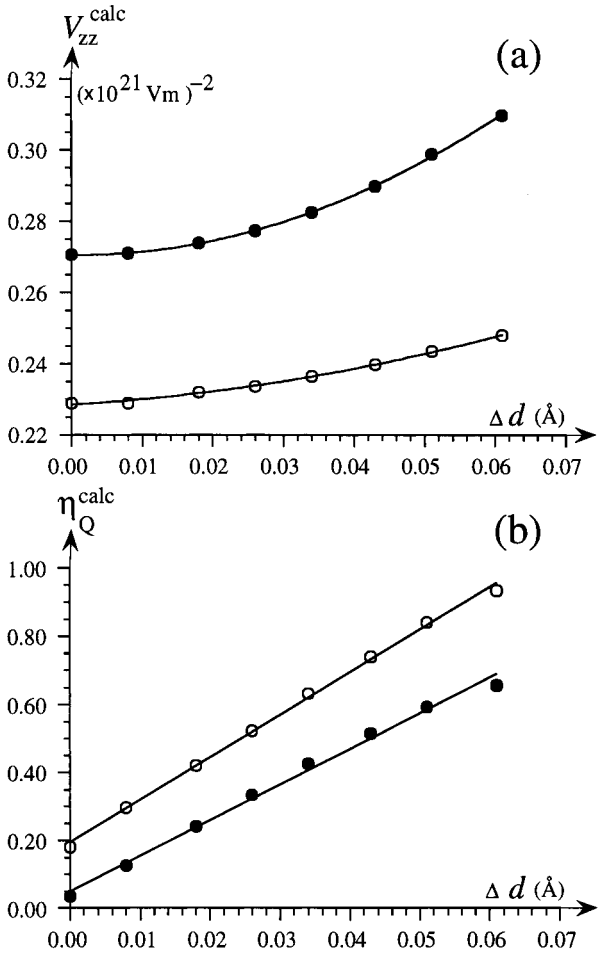

Figure 6. Graphs illustrating (a) the principal element of the ^{27}Al EFG tensor (V_{zz}^{calc}) and (b) the EFG asymmetry parameter (η_Q^{calc}) from point-monopole calculations as a function of the difference in O−H bond length ($\Delta d = d_{O3-H3} - d_{O2-H2}$) for the O3−H3 and O2−H2 hydroxyl groups bonded to aluminum in the α form of Friedels salt. The filled and open circles correspond to calculations for an AlO_6 unit and a cluster of 74 atoms, respectively (see text).

Conclusions

Variable-temperature (VT) ^{27}Al MAS NMR of the central and satellite transitions is shown to be a valuable tool in the characterization of the structural phase transition for Friedels salt ($Ca_2Al(OH)_6Cl\cdot 2H_2O$). The ^{27}Al quadrupole coupling parameters (C_Q and η_Q) are very sensitive to the structural changes induced by the α−β phase transition, while a value independent of temperature is observed for the isotropic chemical shift. The parabolic decrease in C_Q and increase in η_Q with increasing temperature observed for the α phase and the corresponding temperature dependencies of the principal elements of the ^{27}Al quadrupole coupling tensor are not only a result of thermal expansion but reflect the fact that other effects such as thermal vibrations, motions, or rearrangements of the ions have a marked influence on the ^{27}Al electric-field gradient (EFG) tensor. The examination of the O−H bonds in the α and β forms combined with point-monopole calculations of the ^{27}Al EFG tensors, employing large clusters of atoms for the aluminum environment, strongly suggests that hydrogen bonding, reflected by a change in O−H distances for the hydroxyl groups, plays a decisive role for the structural changes that occur

during the $\alpha-\beta$ phase transition. Overall, the present results show great potential for ^{27}Al VT MAS NMR as a tool in the characterization of phase transitions for other lamellar calcium aluminate hydrates.

Acknowledgment. The use of the facilities at the Instrument Centre for Solid-State NMR Spectroscopy, University of Aarhus, sponsored by the Danish Research Councils (SNF and STVF), Teknologistyrelsen, Carlsbergfondet, and Direktør Ib Henriksens Fond, is acknowledged. We thank the Danish Natural Science Research Council (SNF) and Carlsbergfondet for grants to the development of variable-temperature NMR equipment. Financial support from the two Danish Research Councils (J.nr. 2020-00-0018 and J.nr. 0001237) is acknowledged.

References and Notes

(1) Neville, A. *Mater. Struct.* **1995**, *28*, 63.
(2) Justnes, H. *Nord. Concr. Res.* **1998**, *21*, 48.
(3) Suryavanshi, A. K.; Scantlebury, J. D.; Lyon, S. B. *Cem. Concr. Res.* **1996**, *26*, 717.
(4) Glasser, F. P.; Kindness, A.; Stronach, S. A. *Cem. Concr. Res.* **1999**, *29*, 861.
(5) Tang, L.; Nilsson, L.-O. *Cem. Concr. Res.* **1993**, *23*, 247.
(6) Birnin-Yauri, U. A.; Glasser, F. P. *Cem. Concr. Res.* **1998**, *28*, 1713.
(7) Terzis, A.; Filippakis, S.; Kuzel, H.-J.; Burzlaff, H. *Z. Kristallogr.* **1987**, *181*, 29.
(8) Renaudin, G.; Kubel, F.; Rivera, J.-P.; Francois, M. *Cem. Concr. Res.* **1999**, *29*, 1937.
(9) Ahmed, S. J.; Taylor, H. F. W. *Nature* **1967**, *215*, 622.
(10) Renaudin, G.; François, M. *Acta Crystallogr.* **1999**, *C55*, 835.
(11) François, M.; Renaudin, G.; Evrard, O. *Acta Crystallogr.* **1998**, *C54*, 1214.
(12) Burns, G. *J. Chem. Phys.* **1960**, *32*, 1585.
(13) Weiden, N.; Weiss, A. *Ber. Bunsen-Ges. Phys. Chem.* **1975**, 79, 557.
(14) Weiden, N.; Weiss, A. *J. Magn. Reson.* **1975**, 20, 279.
(15) Burum, D. P.; Macfarlane, R. M.; Shelby, R. M.; Mueller, L. *Phys. Lett.* **1982**, *91A*, 465.
(16) Phillips, B. L.; Thompson, J. G.; Xiao, Y.; Kirkpatrick, R. J. *Phys. Chem. Miner.* **1993**, *20*, 341.
(17) Kim, I. G.; Yeom, T. H.; Choh, S. H.; Hong, K. S.; Yu, Y. M.; Choi, E. S. *Solid State Commun.* **2000**, *114*, 311.
(18) Stebbins, J. F. *Chem. Rev.* **1991**, *91*, 1353.
(19) Massiot, D.; Trumeau, D.; Touzo, B.; Farnan, I.; Rifflet, J.-C.; Douy, A.; Coutures, J- P. *J. Phys. Chem.* **1995**, *99*, 16455.
(20) Schønwandt, B. V.; Jakobsen, H. J. *J. Solid State Chem.* **1999**, *145*, 10.
(21) Bielecki, A.; Burum, D. P. *J. Magn. Reson. Ser. A.* **1995**, *116*, 215.
(22) Skibsted, J.; Nielsen, N. C.; Bildsøe, H.; Jakobsen, H. J. *J. Magn. Reson.* **1991**, *95*, 88; *Chem. Phys. Lett.* **1992**, *188*, 405.
(23) Skibsted, J.; Vosegaard, T.; Bildsøe, H.; Jakobsen, H. J. *J. Phys. Chem.* **1996**, *100*, 14872.
(24) Kirkpatrick, R. J.; Yu, P.; Hou, X.; Kim, Y. *Am. Miner.* **1999**, *84*, 1186.
(25) Kushida, T.; Benedek, G. B.; Bloembergen, N. *Phys. Rev.* **1956**, *104*, 1364.
(26) Skibsted, J.; Jakobsen, H. J. *J. Phys. Chem. A* **1999**, *103*, 7958.
(27) Koller, H.; Engelhardt, G.; Kentgens, A. P. M.; Sauer, J. *J. Phys. Chem.* **1994**, *98*, 1544.
(28) Skibsted, J.; Jacobsen, C. J. H.; Jakobsen, H. J. *Inorg. Chem.* **1998**, *37*, 3083.
(29) Sternheimer, R. M. *Phys. Rev.* **1966**, *146*, 140.
(30) Coppens, P. *X-ray charge densities and chemical bonding*; Oxford University Press: Oxford, U.K., 1997.
(31) Lager, G. A.; Von Dreele, R. B. *Am. Miner.* **1996**, *81*, 1097.
(32) Brown, I. D.; Shannon, R. D. *Acta Crystallogr.* **1973**, *A29*, 266.
(33) Brown, I. D.; Altermatt, D. *Acta Crystallogr.* **1985**, *B41*, 244.